Hindawi
Geofluids
Volume 2019, Article ID 3920414, 9 pages
https://doi.org/10.1155/2019/3920414

Research Article

Experimental Investigation of Water-Inrush Risk Based on Permeability Evolution in Coal Mine and Backfill Prevention Discussion

Meng Li,[1] Jixiong Zhang,[1] Weiqing Zhang,[1] Ailing Li,[1] and Wei Yin[2]

[1]*State Key Laboratory of Coal Resources and Safe Mining, School of Mines, China University of Mining & Technology, Xuzhou 221116, China*
[2]*Faculty of Transportation Engineering, Huaiyin Institute of Technology, Huaian 223003, China*

Correspondence should be addressed to Weiqing Zhang; wq.zhang@cumt.edu.cn

Received 10 July 2019; Revised 14 November 2019; Accepted 25 November 2019; Published 30 December 2019

Academic Editor: Stefano Lo Russo

Induced by coal mining, the fractures constantly occur in geologic strata until failure occurs, which provide channels for water flow. Therefore, it is essential to investigate the permeability evolution of rocks under load. Borehole sampling was conducted in a bedrock layer beneath an aquifer, and the permeability evolution of sandstone specimens under different confining pressures was tested in rock mechanics testing laboratories. The results indicated that the permeability gradually decreases with the increasing confining pressures, while the peak strength increases with the increase of confining pressures. The minimum and maximum permeabilities occurred in the sandstone specimens that were subjected to elastic deformation and strain-softening stages, respectively. The failure, and maximum permeability, of these sandstone specimens did not occur simultaneously. To prevent the flow channel being formed due to the development and failure of rock fractures, a method of backfill gob was proposed and also the influence of backfill on fracture development was discussed.

1. Introduction

During coal mining, the strata motion occurs beneath the effect of mine ground pressures which further produce fractures [1–3]. In this context, the water-conducting channels are formed once the fractures are connected with each other so that water in an aquifer flows to the mined panel, which causes a water inrush [4, 5]. In recent years, there have been many water-inrush accidents beneath an aquifer caused by coal mining, which lead to economic loss and threaten safe production in coal mines [6, 7]. Moreover, fractures are constantly being developed and extended, while permeability also varies under the effect of mining-induced stress. Therefore, it is necessary to explore the evolution of permeability in rocks during deformation failure which can provide experimental data revealing the mechanism of water inrush of coal seams beneath an aquifer.

Researchers have carried out plenty of studies on the permeability of coals and rocks by experimental [8–12] and numerical methods [13–15]. Coli et al. [16] presented a new practical technical approach for the evaluation of hydraulic conductivity and tunnel water inflow in complex fractured rock masses, which was used to evaluate water flow into tunnels planned along the new highway project. Bukharov and Ilyushin [17] proposed a method for determining permeability of fractures in hard rocks in seepage problems in dams, and Zhang et al. [18] investigated the relationships between deformation and permeability of brittle rocks. Parisa [19] estimated the permeability of rocks by using a neural network model; Wang et al. [20] studied the characteristic of gas permeability of low-permeability rocks by applying a triaxial test, which provides guidance when constructing underground oil storage facilities. Guo et al. [21] suggested that the permeability of rocks is positively correlated with temperature and pressure after studying the influence of temperature on the permeability of rocks. Meng and Li [22] examined changes in the permeability of high-quality coal. Głowacki and Selvadurai [23] tested the

permeability of limestone under different stresses and proposed an empirical spatial model of permeability evolution. The researches on the permeability evolution in rocks during seepage process can greatly contribute to reveal the seepage mechanism of rocks.

Besides, the water inrush induced by coal mining usually occurs because of the strata breakage during coal mining, which will form the seepage channel for the underground water. For this problem, some methods were proposed to control the water inrush in coal mining; also, the good application effects have been obtained on site. Li et al. [24] discovered a water-inrush mechanism suitable for specific geological and hydrogeological conditions and applied the grouting control measures. In order to prevent the water inrush in coal mine, Wu et al. [25] proposed the vulnerability index approach by coupling the analytic hierarchy process and geographic information system for evaluating the water-inrush risk. Moreover, the coal seams under built-up structures and especially beneath water bodies can be extracted through proper planning for the optimization of coal recovery and systematic strata control investigations [26]. However, the above control methods could not guarantee the strata integrity during coal mining, which will destroy the ecological environment and underground water. Meanwhile, little research is available on combining the rock seepage and the mechanism of water inrush, with a lack of focus to date on permeability evolution in bedrock beneath an aquifer.

Therefore, this study is aimed at investigating the water seepage mechanism of rock strata and proposing the effective control method. Borehole sampling was conducted in bedrock beneath an aquifer to test the permeability evolution of rock specimens under different confining pressures and reveal the causes of water inrush in mining seams therein. Through experimental study on the rock seepage, the relationships between the permeability evolution and failure process of rock can be obtained accurately. Finally, a backfill control method for preventing water-inrush-induced disasters in coal mines was suggested and discussed.

2. Experimental Details

2.1. Experimental Material. The sandstone specimens were taken from the bedrock layer of backfill panel of coal mine in Anhui Province, China. The coal mining of this mine was significantly influenced by an aquifer, because the quaternary aquifer on the bottom of the unconsolidated formation directly overlaid the bedrock layer, below which there is no aquiclude. Moreover, the minimum distance between the coal seam of backfill panel and the aquifer was 21.8 m. The coal seam is affected by the aquifer, and it cannot be excavated by the conventional mining method. The thickness of the aquifer ranges from 6.12 to 39.19 m with an average of 20.7 m, and it contains materials including gravels, grits, clayey gravels, coarse sands, medium sands, and clayed sands. The immediate roof is comprised of siltstone and fine sandstone with high associated wet and dry strengths and a mean thickness of 5.8 m. Core drilling was conducted in a backfill panel to test the seepage characteristics of the bedrock, providing experimental data aimed at preventing future water-inrush risk caused by coal mining beneath an aquifer. The minerals in this sandstone mainly include feldspar, quartz, kaolinite, illite, and chlorite. It has an average density of 2570 kg/m^3. Cylindrical specimens measuring 50 mm in diameter, and 100 mm in height, were cut from bulk specimens.

By using a scanning electron microscope (SEM), the microstructures of the sandstone specimens after 260x, 1400x, and 2400x magnification were obtained, as shown in Figure 1. Most mineral particles appear as irregular blocks, and they are interconnected; however, there are microscopic defects in the mineral particles including micropores and microcracks. The micropores and microcracks exhibit lower tensile and compressive strengths compared with the intact rock, and they are considered as having formed the original seepage channels allowing constant fluid flow in the specimens [27].

2.2. Experimental Apparatus and Test Method. The seepage characteristics of the sandstone specimens were tested by using a computer-controlled MTS815.03 test system. The maximum axial load was 4600 kN. As shown in Figure 2, both upper and lower ends of each specimen were capped by a porous steel plate to ensure a uniform water pressure was imposed over the whole specimen cross-section and to guarantee uniform liquid penetration to the specimen from its end surfaces. The upper and lower water pressures were separately imposed on the upper and lower porous plates of the specimen. A vertical hole was separately made in the centre of the porous plates so that the flow channel for water was formed. A plastic insulation sleeve, and a heat-shrinkable plastic sleeve, was used to seal the specimen.

The basic mechanism of the seepage experiment is shown as follows: axial pressure P_1, confining pressure P_2, and pore pressure P_3 were imposed (keeping $P_3 < P_2$) and then pore pressure P_4, at the lower end of specimen, was decreased so that the difference in osmotic pressure ($\triangle P = P_3 - P_4$) can be established across the two ends of the specimen. Thus, water was forced into the specimen.

To investigate the influence of stress on the seepage characteristics of sandstones at different burial depths, the seepage characteristics of sandstone specimens under confining pressures of 4, 6, 8, and 10 MPa were separately measured. Moreover, the axial stress was imposed on the specimen, and then, the permeability k of the specimen was calculated by using the following formula [28, 29]:

$$k = \frac{1}{5n}\sum_{i=1}^{n} 526 \times 10^{-6} \times \lg\left[\frac{\Delta P(i-1)}{\Delta P(i)}\right], \quad (1)$$

where n, $\Delta P(i-1)$, and $\Delta P(i)$ refer to line numbers of data acquisition, and differences in osmotic pressures between the $(i-1)$th and ith lines, respectively.

Before conducting the seepage experiment, it is necessary that the specimen was fully saturated in advance because the seepage process was blocky if the specimen was partially saturated; moreover, the cylindrical sandstone specimens

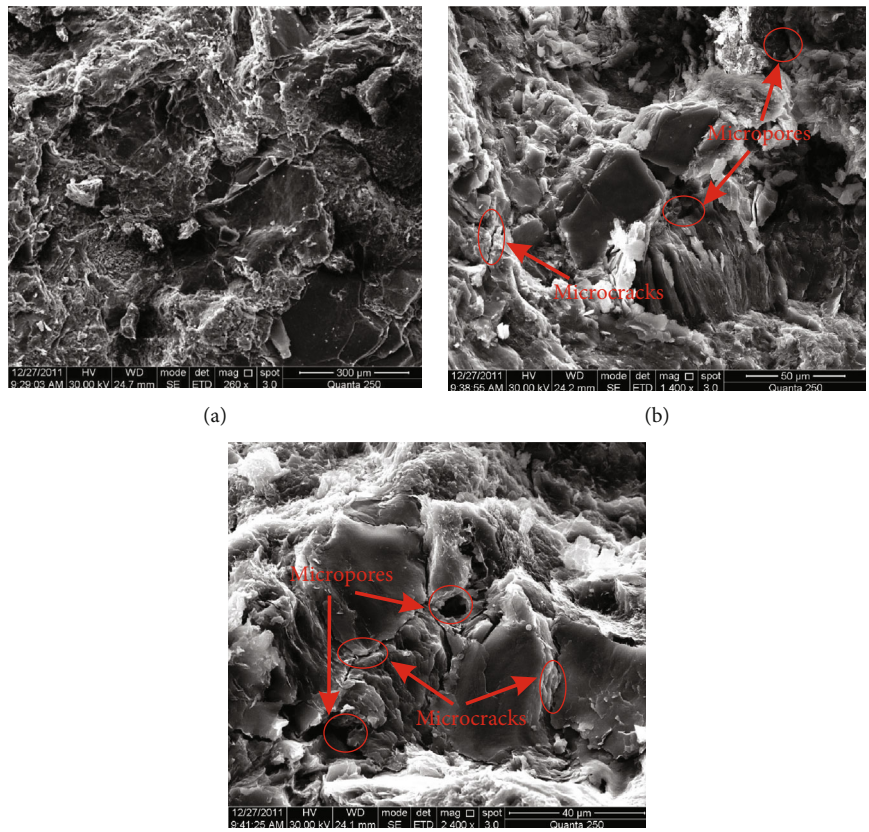

Figure 1: Microstructures of sandstones obtained by SEM. (a) 260x; (b) 1400x; (c) 2400x.

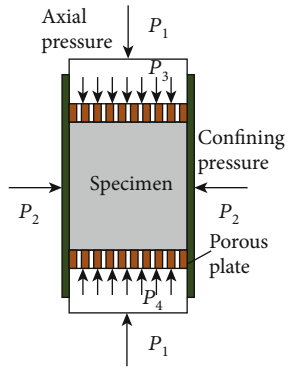

Figure 2: The schematic diagram for testing the seepage characteristics of rock specimens.

were sealed during testing, or water inside the specimen was mixed with oil inside the triaxial cell itself.

3. Analysis of Experimental Results

The relationships between the axial stress and permeability with the axial strain in the sandstone under different confining pressures is shown in Figure 3: it was similar to that between the permeability and axial strain under different confining pressures. Under different confining pressures, primary microcracks and micropores were in a densification and closure stage before the sandstone specimens reached the elastic limit under constantly increasing stress. Moreover, there was a linear relationship between the axial stress and strain: after this elastic deformation, new fractures in the sandstone specimens developed and extended so that plastic deformation occurred. After the sandstone specimens reached their peak strength, the stresses rapidly decreased, showing strain-softening. Thereafter, the sandstone specimens dilated further until reaching their residual strength.

Owing to primary micropores and microcracks in the sandstone specimens becoming densified and more tightly closed as stresses increased in the elastic deformation stage, the permeability decreased rapidly. In the plastic deformation stage, new fractures rapidly developed and extended and the permeability gradually increased after the sandstone specimens reached their ultimate strength. And then the permeability reached its maximum value after the sandstone specimens were damaged. Moreover, new fractures were constantly being developed in the sandstone specimens and eventually failure occurred, which can constantly provide channels for water flow.

Figure 3 shows that the minimum and maximum permeability occurred when the sandstone specimens were subjected to the elastic deformation stage and in the strain-softening stage. Moreover, the maximum permeability occurred after the sandstone specimens reached peak

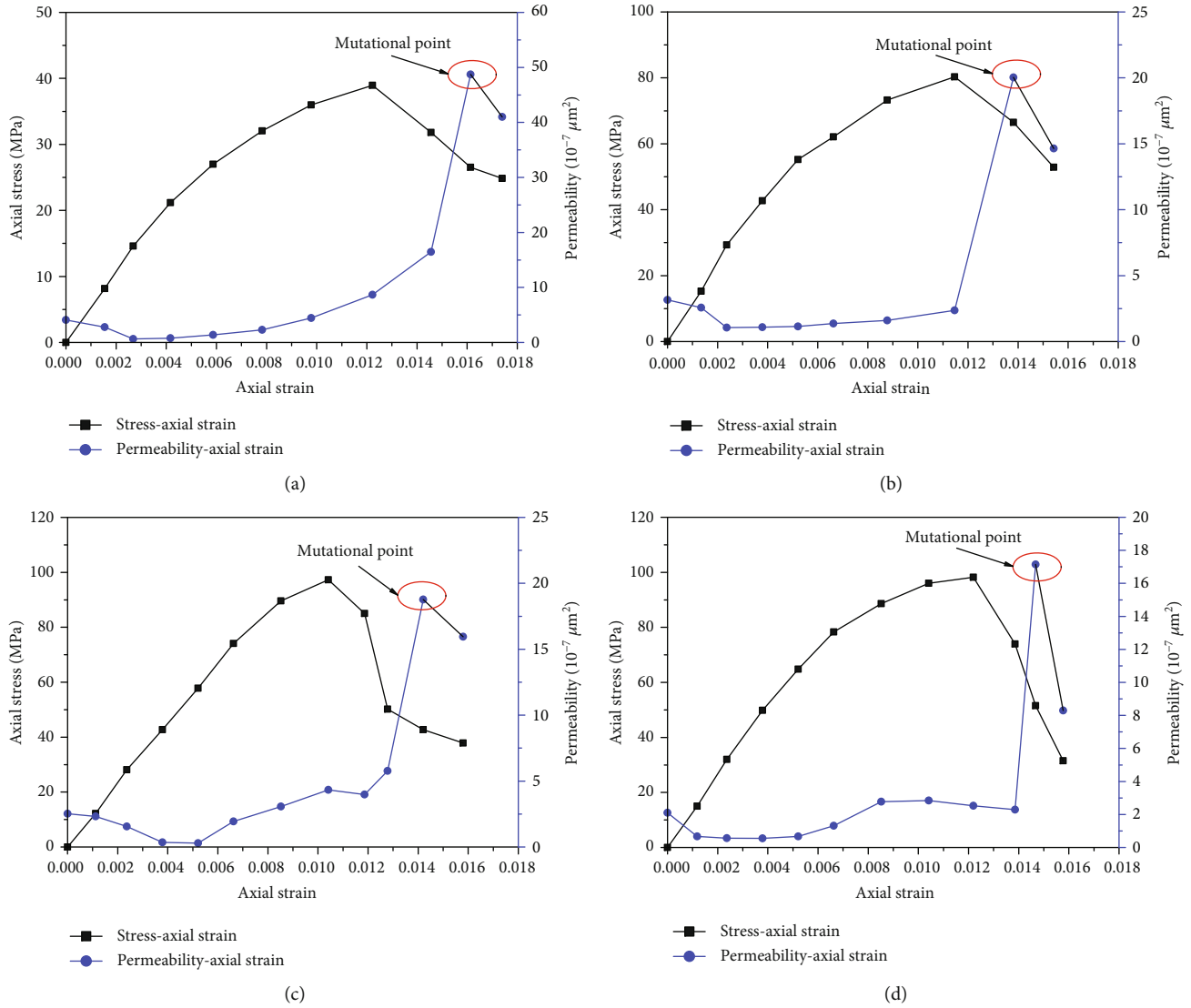

Figure 3: The relationships between stress, permeability, and axial strain under different confining pressures. (a) 4 MPa; (b) 6 MPa; (c) 8 MPa; (d) 10 MPa.

strength, implying that the failure of the sandstone specimens did not simultaneously appear upon attainment of the maximum permeability. The permeability suddenly reached a maximum after the sandstone specimens were completely damaged. During coal mining, a channel for water flow was formed due to the mutation allowing water flow to the panel so that coal mines were subjected to water-inrush-induced disaster, threatening the safe mining of coal.

The relationship between the maximum permeability and peak strength of sandstone with confining pressures is shown in Figure 4. The maximum permeability gradually decreased with increasing confining pressure while the peak strength rose with increasing confining pressures. When the confining pressure increased from 4 MPa to 10 MPa, the maximum permeability of the specimen fell from 48.7×10^{-7} μm^2 to 17.1×10^{-7} μm^2 while the peak strength increased from 38.9 MPa to 98.2 MPa.

4. Discussions

According to the relationships between the stress and the permeability, the process from deformation to failure can be divided into six stages (Figure 5) [30, 31]. The six stages include the closure of microcracks (OA), an elastic deformation stage (AB), a fracture-development and extension stage (BC), rapid development to instability of fracture (CD), a strain-softening stage (DE), and a residual strength stage (EF).

Along OA, the primary cracks were compressed and further closed so that the void volume of the specimen reduced and the permeability decreased overall. During the elastic deformation stage (AB), the strain gradually decreased with increasing stress. Moreover, there was an approximately linear relationship between the axial stress and strain and the permeability of the specimen increased gradually. During the development and extension of cracks (BC), the specimen

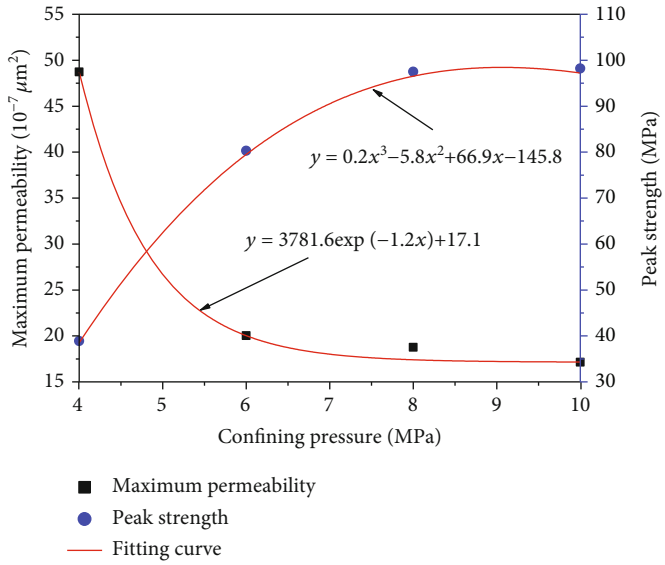

Figure 4: The relationships between maximum permeability and peak strength of sandstones and confining pressure.

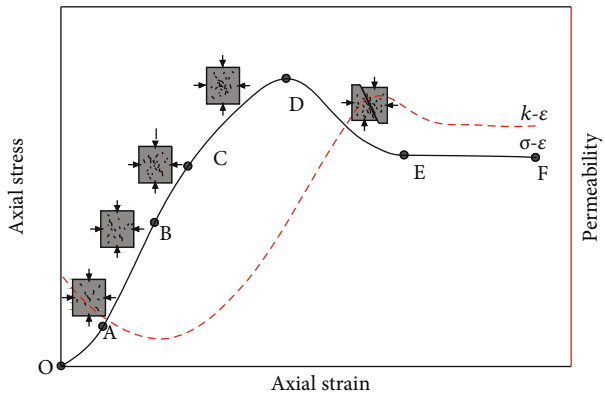

Figure 5: The relationships between stress, permeability, and strain in these sandstone specimens.

was subject to the plastic deformation after it reached the elastic limit and new fractures and joints appeared with increasing stress, causing the permeability to increase rapidly. Afterwards, the fractures rapidly developed during the instability stage (CD). During this stage, fractures and joints in the specimen rapidly developed and extended after the specimen reached the yield limit until the specimens were completely damaged and the permeability increased significantly. During the strain-softening stage (DE), the fractures and joints inside the specimens were gradually damaged after the specimen reached the peak strength and the stress gradually reduced to a stable value (residual strength) with increasing stress. Moreover, the permeability rapidly rose to its maximum after the specimen reached peak strength. During stage (EF), after the specimen was subjected to strain-softening, the stress and permeability changed a little with increasing strain.

A water inrush in this coal mine is shown in Figure 6. After the coal was mined, the immediate roof collapsed to form a caving zone under the effect of the pressure from overlying strata due to loss of support from the lower coal seam. In contrast, the main roof gradually moved towards the lower part of the seam and the fractures gradually extended and ruptured when the internal stress reached the ultimate strength. Moreover, the rupture developed along the overlying strata to form a fractured zone. The caving and fractured zones formed the water-conducting fractured zone. Once the water-conducting fractured zone developed to the aquifer, the water flowed to the panel through the connected fractures induced by coal mining, which caused the aforementioned water inrush.

It can be seen from the experimental results in Section 3 that the overlying strata gradually sank after the coal seam was mined and fractures inside the strata gradually developed and eventually ruptured under the effect of stresses induced by coal mining. As the strata at each layer were damaged, the fracture meshes were formed, which were thus porous. Water in the aquifer can flow into the mining panel through the fractures, and a water inrush ensued.

Through the above analysis, it can be speculated that it is necessary to control the fracture meshes in strata so as not to form a connection with an aquifer, and to prevent water-inrush-induced disasters. Therefore, the gob of the panel can be backfilled by using backfill materials after coal seams was mined so that the room left due to coal mining can be backfilled, and the backfill materials (as the main support) were used to bear the loads of overlying strata, which effectively constrained the subsidence of the roof [32–34]. Thus, overlying strata were mainly expressed as curved subsidence and fractures in limited areas, which effectively decreased the height of the water-conducting fractured zone and guaranteed the safe mining of coal seam beneath an aquifer [35].

It has been proposed that solid wastes (gangues, coal ash, and slag) are backfilled into the gob to control the strata movement and fracture development [36, 37]; the method

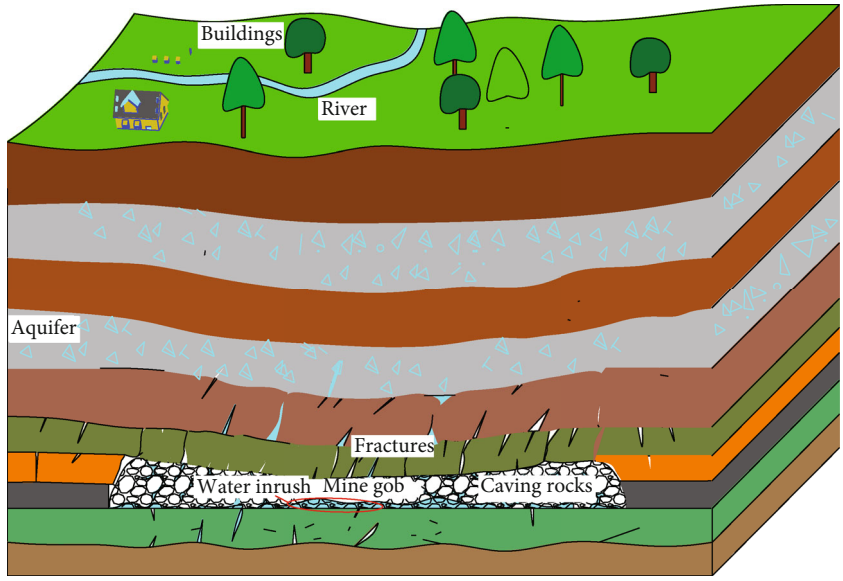

Figure 6: Water inrush in a coal mine induced by an aquifer.

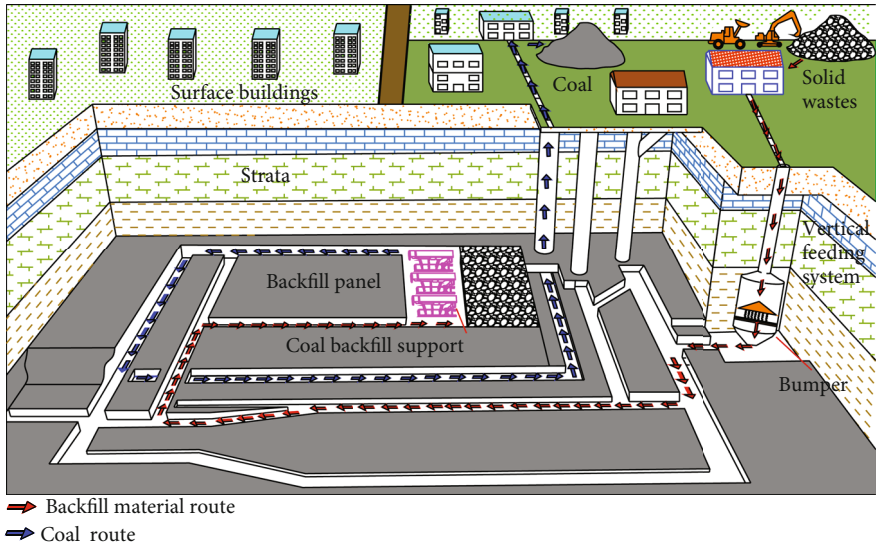

Figure 7: The method schematic of solid backfill mining in a coal mine.

schematic of solid backfill mining is shown in Figure 7. To investigate the development of the water-conducting fractured zone in overlying strata during solid backfill mining, the relationships of mining height and compression ratio to the height of the water-conducting fractured zone are obtained through regression using SPSS statistical analysis software [35, 38]:

$$H_{li} = 31.96 + 2.72M - 34.56\varphi, \tag{2}$$

where H_{li} refers to the height of water-conducting fractured zone, φ is the compression ratio, and M is the mining height.

While the compression ratio represents the ratio of the final subsidence of the roof to the mining height, the larger the compression ratio, the better the backfilling effect.

$$\varphi = \frac{M - M_e}{M}, \tag{3}$$

where M_e refers to the final subsidence of the roof.

According to Formula (2), the relationships of the mining height and the compression ratio to the height of the water-conducting fractured zone are derived, as shown in Figure 8.

As shown in Figure 8, the lower the mining height, the larger the compression ratio and the lower the height of the water-conducting fractured zone. Therefore, for those geological conditions specific to this coal mine, the compression

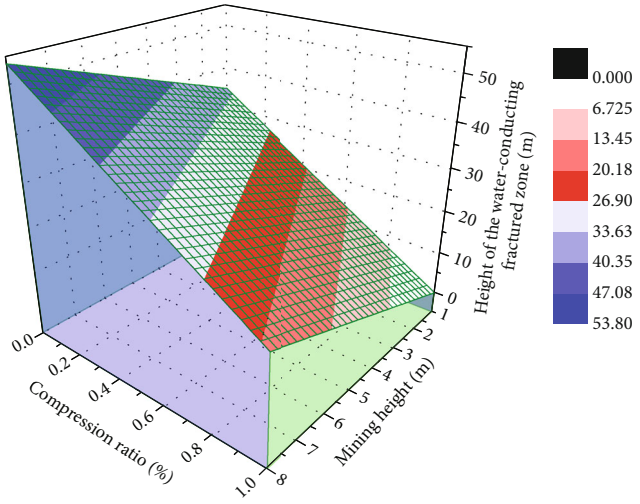

Figure 8: The relationships of the height of water-conducting fractured zone to the mining height and compression ratio.

ratio is a crucial factor in controlling the height of the water-conducting fractured zone. Moreover, the larger the compression ratio, the better the backfill effect and the less the subsidence of overlying strata, and therefore, the water-conducting fractured zone does not reach the aquifer, thus reducing the risk of a water inrush.

In order to monitor the height of the water-conducting fractured zone during the mining of backfill panel, two monitoring boreholes were drilled and installed above the backfill panel. Drilling fluid was used to monitor the fracture development of the strata. The depths of both borehole 1 and borehole 2 were 295.0 m, and the end hole was at the floor strata of the coal seam. After mining the backfill panel, the displacement and deformation of strata were relatively moderate, and the development height of fractures was approximately 10.0 m. Also, the height of the water-conducting fractured zone did not develop to the aquifer. The monitoring results show that adopting the backfill method can effectively reduce the development height of the water-conducting fractured zone in strata beneath an aquifer to achieve safer mining.

5. Conclusions

This paper is aimed at investigating the permeability changes in rocks during loading and revealing the mechanism of water inrush in coal mining beneath an aquifer. To achieve this aim, borehole sampling was conducted on the bedrock layer beneath the aquifer and the permeability evolution of the sandstone specimens under different confining pressures was investigated.

Owing to the primary micropores and microcracks in the sandstone specimens being densified and further closed as the stress increased in the elastic deformation stage, the permeability decreased rapidly. In the plastic deformation stage, new fractures developed and extended rapidly: the permeability gradually increased after the sandstone specimens reached ultimate strength, and then, the permeability suddenly reached its maximum value after the sandstone specimens were completely damaged. Moreover, the minimum and maximum permeabilities occurred when the sandstone specimens were subject to elastic deformation and in the strain-softening stage. Additionally, the maximum permeability appeared after the sandstone specimens reached their peak strength, implying that failure of the sandstone specimens did not occur at the same time as the maximum permeability was reached.

The permeability suddenly reached its maximum value after the sandstone specimens were completely damaged. During coal mining, a channel for water flow was formed due to the mutation which allowed water to flow to the panel and cause a water inrush. The backfill method can be used to reduce the fracture development induced by coal mining and prevent the water-conducting fractured zone from reaching the aquifer, thus reducing the risk of a water inrush.

Data Availability

The data used to support the findings of this study are included within the article.

Conflicts of Interest

The authors declare that they have no conflicts of interest.

Acknowledgments

Financial support for this work provided by the National Postdoctoral Program for Innovative Talents (BX20180361), the National Science Fund for Distinguished Young Scholars (51725403), the Independent Research Project of State Key Laboratory of Coal Resources and Safe Mining, CUMT (SKLCRSM19X001), and the Natural Science Foundation of Colleges in Jiangsu Province (KJB440004) is gratefully acknowledged.

References

[1] J. Cao and W. P. Li, "Numerical simulation of gas migration into mining-induced fracture network in the goaf," *International Journal of Mining Science and Technology*, vol. 27, no. 4, pp. 681–685, 2017.

[2] V. Palchik, "Formation of fractured zones in overburden due to longwall mining," *Environmental Geology*, vol. 44, no. 1, pp. 28–38, 2003.

[3] J. Pan, M. Lv, Q. Hou, Y. Han, and K. Wang, "Coal microcrystalline structural changes related to methane adsorption/-desorption," *Fuel*, vol. 239, pp. 13–23, 2019.

[4] D. Ma, H. Bai, and Y. Wang, "Mechanical behavior of a coal seam penetrated by a karst collapse pillar: mining-induced groundwater inrush risk," *Natural Hazards*, vol. 75, no. 3, pp. 2137–2151, 2015.

[5] S. Zhang, W. Guo, Y. Li, W. Sun, and D. Yin, "Experimental simulation of fault water inrush channel evolution in a coal mine floor," *Mine Water and the Environment*, vol. 36, no. 3, pp. 443–451, 2017.

[6] J. C. Zhang and B. H. Shen, "Coal mining under aquifers in China: a case study," *International Journal of Rock Mechanics and Mining Sciences*, vol. 41, no. 4, pp. 629–639, 2004.

[7] J. Wu, S. Xu, R. Zhou, and Y. Qin, "Scenario analysis of mine water inrush hazard using Bayesian networks," *Safety Science*, vol. 89, pp. 231–239, 2016.

[8] H. Meng and T. Y. Liu, "Interpretation of the rock-electric and seepage characteristics using the pore network model," *Journal of Petroleum Science and Engineering*, vol. 180, pp. 1–10, 2019.

[9] A. Vinsot, Y. Linard, M. Lundy, S. Necib, and S. Wechner, "Insights on desaturation processes based on the chemistry of seepage water from boreholes in the callovo-oxfordian argillaceous rock," *Procedia Earth and Planetary Science*, vol. 7, pp. 871–874, 2013.

[10] J. Liu, J. Gao, X. Zhang, G. Jia, and D. Wang, "Experimental study of the seepage characteristics of loaded coal under true triaxial conditions," *Rock Mechanics and Rock Engineering*, vol. 52, no. 8, pp. 2815–2833, 2019.

[11] K. Peng, X. B. Li, Z. W. Wang, and A. H. Liu, "A numerical simulation of seepage structure surface and its feasibility," *Journal of Central South University*, vol. 20, no. 5, pp. 1326–1331, 2013.

[12] Z. Wang, J. Pan, Q. Hou, B. Yu, M. Li, and Q. Niu, "Anisotropic characteristics of low-rank coal fractures in the Fukang mining area, China," *Fuel*, vol. 211, pp. 182–193, 2018.

[13] M. G. Sweetenham, R. M. Maxwell, and P. M. Santi, "Assessing the timing and magnitude of precipitation-induced seepage into tunnels bored through fractured rock," *Tunnelling and Underground Space Technology*, vol. 65, pp. 62–75, 2017.

[14] Z. Wang, J. Pan, Q. Hou et al., "Changes in the anisotropic permeability of low-rank coal under varying effective stress in Fukang mining area, China," *Fuel*, vol. 234, pp. 1481–1497, 2018.

[15] X. X. Li and D. Q. Li, "A numerical procedure for unsaturated seepage analysis in rock mass containing fracture networks and drainage holes," *Journal of Hydrology*, vol. 574, pp. 23–34, 2019.

[16] N. Coli, G. Pranzini, A. Alfi, and V. Boerio, "Evaluation of rock-mass permeability tensor and prediction of tunnel inflows by means of geostructural surveys and finite element seepage analysis," *Engineering Geology*, vol. 101, no. 3-4, pp. 174–184, 2008.

[17] R. K. Bukharov and F. Ilyushin, "Determination of permeability of cracks in hard rock," *Hydrotechnical Construction*, vol. 25, no. 8, pp. 500–502, 1991.

[18] R. Zhang, Z. Jiang, Q. Sun, and S. Zhu, "The relationship between the deformation mechanism and permeability on brittle rock," *Natural Hazards*, vol. 66, no. 2, pp. 1179–1187, 2013.

[19] B. Parisa, "Committee neural network model for rock permeability prediction," *Journal of Applied Geophysics*, vol. 104, no. 5, pp. 142–148, 2014.

[20] H. Wang, W. Xu, J. Shao, and F. Skoczylas, "The gas permeability properties of low-permeability rock in the process of triaxial compression test," *Materials Letters*, vol. 116, no. 2, pp. 386–388, 2014.

[21] X. Guo, G. Zou, Y. Wang, Y. Wang, and T. Gao, "Investigation of the temperature effect on rock permeability sensitivity," *Journal of Petroleum Science and Engineering*, vol. 156, pp. 616–622, 2017.

[22] Z. Meng and G. Li, "Experimental research on the permeability of high-rank coal under a varying stress and its influencing factors," *Engineering Geology*, vol. 162, no. 14, pp. 108–117, 2013.

[23] A. Głowacki and A. P. S. Selvadurai, "Stress-induced permeability changes in Indiana limestone," *Engineering Geology*, vol. 215, pp. 122–130, 2016.

[24] B. Li, H. B. Bai, and J. J. Wu, "Mechanism of water inrush driven by grouting and control measures—a case study of Chensilou mine, China," *Arabian Journal of Geosciences*, vol. 10, pp. 1–10, 2017.

[25] Q. Wu, Y. Liu, D. Liu, and W. Zhou, "Prediction of floor water inrush: the application of gis-based ahp vulnerable index method to Donghuantuo coal mine, China," *Rock Mechanics and Rock Engineering*, vol. 44, no. 5, pp. 591–600, 2011.

[26] A. Gandhe, V. Venkateswarlu, and R. N. Gupta, "In situ investigations into overburden failures of a super-thick coal seam for longwall top coal caving," *Rock Mechanics and Rock Engineering*, vol. 78, no. 5, pp. 155–162, 2005.

[27] S. Q. Yang, Y. H. Huang, Y. Y. Jiao, W. Zeng, and Q. L. Yu, "An experimental study on seepage behavior of sandstone material with different gas pressures," *Acta Mechanica Sinica*, vol. 31, no. 6, pp. 837–844, 2015.

[28] L. Shiping, L. Yushou, L. Yi, W. Zhenye, and Z. Gang, "Permeability-strain equations corresponding to the complete stress–strain path of Yinzhuang Sandstone," *International journal of rock mechanics and mining sciences & geomechanics abstracts*, vol. 31, no. 4, pp. 383–391, 1994.

[29] S. Peng, Z. Meng, H. Wang, C. Ma, and J. Pan, "Testing study on pore ratio and permeability of sandstone under different confining pressures," *Chinese Journal of Rock Mechanics and Engineering*, vol. 22, no. 5, pp. 742–746, 2003.

[30] Z. P. Meng, B. Y. Wang, L. W. Xu, Z. Y. Wu, G. Bai, and B. T. Lu, "Influence of coal mining on the deformation-failure and permeability of seam floor," *Coal Geology & Exploration*, vol. 40, no. 2, pp. 39–43, 2012.

[31] Z. P. Meng, J. Zhang, X. C. Shi, Y. D. Tian, and C. Li, "Calculation model of rock mass permeability in coal mine goaf and its numerical simulation analysis," *Journal of China Coal Society*, vol. 41, no. 8, pp. 1997–2005, 2016.

[32] X. J. Zhu, G. L. Guo, and Q. Fang, "Coupled discrete element–-finite difference method for analyzing subsidence control in fully mechanized solid backfilling mining," *Environmental Earth Sciences*, vol. 75, no. 8, 2016.

[33] M. Junker and H. Witthaus, "Progress in the research and application of coal mining with stowing," *International Journal of Mining Science and Technology*, vol. 23, no. 1, pp. 7–12, 2013.

[34] M. Li, J. Zhang, W. Song, and D. M. Germain, "Recycling of crushed waste rock as backfilling material in coal mine: effects of particle size on compaction behaviours," *Environmental Science and Pollution Research*, vol. 26, no. 9, pp. 8789–8797, 2019.

[35] M. Li, J. X. Zhang, X. J. Deng, N. Zhou, and Q. Zhang, "Method of water protection based on solid backfill mining under water bearing strata and its application," *Journal of China Coal Society*, vol. 42, no. 1, pp. 127–133, 2017.

[36] B. Li and F. Ju, "An experimental investigation into the compaction characteristic of granulated gangue backfilling materials modified with binders," *Environmental Earth Sciences*, vol. 77, no. 7, 2018.

[37] J. Li, Y. Huang, Z. Chen, J. Zhang, H. Jiang, and Y. Zhang, "Characterizations of macroscopic deformation and particle crushing of crushed gangue particle material under cyclic loading: in solid backfilling coal mining," *Powder Technology*, vol. 343, pp. 159–169, 2019.

[38] J. Zhang, H. Jiang, X. Deng, and F. Ju, "Prediction of the height of the water-conducting zone above the mined panel in solid backfill mining," *Mine Water and the Environment*, vol. 33, no. 4, pp. 317–326, 2014.